Biochemistry and Biophysics Reports 8 (2016) 284–289

Contents lists available at ScienceDirect

Biochemistry and Biophysics Reports

journal homepage: www.elsevier.com/locate/bbrep

First attempts to crystallize a non-homogeneous sample of thioredoxin from *Litopenaeus vannamei*: What to do when you have diffraction data of a protein that is not the target?

Adam A. Campos-Acevedo[a,*], Adelaida Díaz-Vilchis[a], Rogerio R. Sotelo-Mundo[b], Enrique Rudiño-Piñera[a,*]

[a] *Departamento de Medicina Molecular y Bioprocesos, Instituto de Biotecnología (IBT), Universidad Nacional Autónoma de México (UNAM), Avenida Universidad 2001, Colonia Chamilpa, PO Box 62210, Cuernavaca, Morelos, Mexico*

[b] *Laboratorio de Estructura Biomolecular, Centro de Investigación en Alimentación y Desarrollo, A. C. (CIAD), Carretera a Ejido La Victoria Km 0.6, PO Box 1735, Hermosillo, Sonora 83304, Mexico*

ARTICLE INFO

Keywords:
Crystal structure
Inorganic pyrophosphatase
Program *BALBES*
Protein crystallization
Protein purity

ABSTRACT

The importance of sample homogeneity and purity in protein crystallization is essential to obtain high-quality diffracting crystals. Here, in an attempt to determine the crystal structure of thioredoxin 1 from whiteleg shrimp *Litopenaeus vannamei* (*Lv*Trx), we inadvertently crystallized the hexameric inorganic pyrophosphatase of *Escherichia coli* (E-PPase) from a non-homogeneous sample product during the initial over-expression steps and partial purification of *Lv*Trx. The structure determination and identification of the crystallized protein were derived from several clues: the failures in the Molecular Replacement (MR) trials using *Lv*Trx coordinates as a search model, the unit cell parameters and space group determination, and essentially by the use of the program *BALBES*. After using the previously deposited E-PPase structure (PDB entry 1mjw) as a search model and the correct space group assignation, the MR showed an E-PPase complexed with SO_4^{-2} with small changes in the sulfate ion binding region when it compares to previously deposited E-PPases in the PDB. This work stresses the importance of protein purity to avoid the risk of crystallizing a contaminant protein or how pure need to be a protein sample in order to increase the possibility to obtain crystals, but also serves as a reminder that crystallization is by itself a purification process and how the program *BALBES* can be useful in the crystal structure determination of previously deposited structures in the PDB.

1. Introduction

To determine the three-dimensional coordinates of proteins by crystallography, it is necessary first to purify and then generate crystals of suitable size and quality for X-ray diffraction experiments. Although significant work has been performed to develop protein crystallization methodologies, protein crystallization remains as a bottleneck for structural determination [1–4]. Purity is the first variable that is essential to accomplish to obtain protein crystals [5–7] since contaminants within a protein batch may alter the crystal packing of a growing crystal [8–10]. Studies on the effect of macromolecular impurities on protein solubility and crystallizability are limited. However, Skouri et al. in 1995 [6] measured the effect of 2% (w/v) ovalbumin on lysozyme solubility over a concentration of 3–8% (w/v) NaCl. They also conducted similar experiments exploring the effect on lysozyme solubility using 1% (w/v) ovalbumin, 1% (w/v) conalbumin, and 1% (w/v) bovine serum albumin. However, no significant effects were observed in the crystalline packing.

Escherichia coli is the most used bacterial expression systems due to the in-depth knowledge of this microorganism and for the high amounts of heterologous proteins that can be produced. However, despite its many advantages, particular conditions such as incubation time or other stresses during the culture stage may favor the expression of *E. coli* native proteins more than the heterologous protein expression. Such is the case of E-PPase expressed in conditions where the energetic source is compromised to keep the culture alive [11]. In this work, we describe the expression, purification, crystallization, structural determination and coordinates analysis of the E-PPase complexed with SO_4^{-2} as a result of crystallization experiments using a non-homogeneous partially purified *Lv*Trx sample.

* Corresponding authors.
E-mail addresses: adam@ibt.unam.mx (A.A. Campos-Acevedo), rudino@ibt.unam.mx (E. Rudiño-Piñera).

http://dx.doi.org/10.1016/j.bbrep.2016.09.011
Received 25 August 2016; Received in revised form 22 September 2016; Accepted 23 September 2016
Available online 15 October 2016

2. Materials and methods

2.1. Expression and purification

The *E. coli* PPase was similarly purified by previously published studies of whiteleg shrimp thioredoxin 1 from *Litopenaeus vannamei* (*Lv*Trx) [11–13]. Cells of the host strain *E. coli* BL21 (DE3) transformed with plasmid pET11a/*Lv*Trx were grown on Luria-Bertani (LB) agar plates [1% (w/w) tryptone, 0.5% (*w/v*) yeast extract, 1% (*w/v*) NaCl] containing 200 μg ml^{-1} ampicillin at 310 K. A single colony was picked and grown for plasmid isolation. A colony was inoculated into 50 ml LB broth containing 200 μg ml^{-1} ampicillin and incubated for 12 h at 310 K; part of the culture (25 ml) was used to inoculate l L of LB medium with 200 μg ml^{-1} ampicillin. The culture was grown to an absorbance of 0.6 at OD_{600}. IPTG (isopropyl-β-thiogalactoside) was added to the broth to a final concentration of 0.4 mM and grown for an additional 12 h. The cells were then harvested by centrifugation (24,000*g*, 30 min, 277 K) using a Beckman JA-14 rotor centrifuge (Beckman Coulter, CA, USA) and washed in 0.9% NaCl (*w/v*). The cells were resuspended in cold lysis buffer (100 mM Tris–HCl, pH 8.0) containing Complete EDTA-free® protease-inhibitor cocktail (Roche Molecular Biochemical, USA) and sonicated with three pulses per 1 min and one rest interval of 5 min per pulse on an ice bath. Cell debris was removed by centrifugation (24,000*g*, 20 min, 277 K), and the supernatant containing the soluble target protein was collected for purification.

The supernatant was fractionated by two consecutive precipitation steps at 50% and 85% ammonium sulfate saturation. The precipitate was resuspended in buffer (10 mM Tris–HCl, pH 7.5) and heated at 343 K for 20 min. Cell debris was then removed by centrifugation (24,000*g*, 20 min, 277 K). The supernatant was dialyzed two times at 277 K in ten times its volume in buffer (10 mM Tris–HCl, pH 7.5) and the supernatant was loaded onto a 15 ml ion exchange column (Q-Sepharose™ GE Healthcare, Sweden) pre-equilibrated and washed with three column volumes of buffer (10 mM Tris–HCl, pH 7.5). The sample was eluted with a pulse of 300 mM NaCl in the same buffer at a flow rate of 1 ml min^{-1}. Column fractions were collected and analyzed by SDS-PAGE, and fractions with the enzyme were pooled and dialyzed against buffer 10 mM Tris–HCl, pH 7.5, and concentrated. Protein concentration was determined with the Bradford dye reagent (Bio-Rad Laboratories, USA) [14].

2.2. Protein crystallization

Crystallization trials were performed using Crystal Screen and Crystal Screen II kits from Hampton Research (Aliso Viejo, CA, USA) by the hanging drop vapor-diffusion method at 291 K. The drops were prepared manually in 24-well crystallization plates by mixing the enzyme (2 μl) at 30 mg ml^{-1} with the reservoir solution (2 μl) containing 0.1 M sodium acetate, pH 4.6 and 2.0 M ammonium sulfate. DTT was added to a final concentration of 5 mM directly in the crystallization drops. Suitable crystals for diffraction were obtained in one month. Crystals for data collection were then flash-cooled by immersion in liquid nitrogen using 30% (v/v) glycerol into the mother solution as a cryoprotectant.

2.3. Data collection and structure determination

Diffraction data were collected on beamline X6A of the National Synchrotron Light Source (NSLS), Brookhaven National Laboratory (BNL), USA, using an ADSC Quantum 270 detector. The X-ray diffraction data were collected from a single crystal at 100 K (incident wavelength, λ=0.975 Å). The diffraction images data were integrated using XDS [15] and scaled with SCALA from the CCP4 suite (Collaborative Computational Project, Number 4) [16]. Molecular replacement was done with a cross-rotational search followed by a translational search using the coordinates of E-PPase was performed using the program PHASER [17] to obtain initial models and phases (LLG=8383, RFZ=9.9, TFZ=11.9, being a trimer found in the asymmetric unit). The models were improved based on manual inspection of the $2F_o–F_c$ map after rigid-body refinement and geometric constraint performed in REFMAC [18]. All further refinement was done using the PHENIX suite [19]. The final model was completed and refined using the programs PHENIX and COOT to a final R_{work}/R_{free} of 19.3/23.5% [20]. Data collection and refinement statistics are summarized in Table 1.

Table 1
Summary of crystallographic data collection and refinement. Values in parentheses are for the highest resolution shell.

Parameters	*E-PPase PDB (4UM4)*
Data collection statistics	
X-ray source	*BNL NSLS Beamline X6A*
Wavelength (Å)	*0.975*
Space group	*C 1 2 1*
Unit-cell dimensions	
a, b, c (Å)	*120.0, 108.9,81.0*
α, β, γ angles (°)	*120.0, 108.9, 81.0*
Resolution range (Å)	*90.0, 97.0, 90.0*
No. de reflections	*19.10–2.65*
No. of unique reflections	*61,030*
Completeness (%)	*27,508*
R_{sym} *(%)*[1]	*92.0 (94.0)*
R_{meas} *(%)*[2]	*6.0 (43)*
I/σ(I)	*7.9 (56)*
Multiplicity	*10.3 (2.3)*
Asymmetric unit content	*2.2 (2.2)*
	Trimer
Refinement statistics	
R_{work}/R_{free} *(%)*	*19.3/23.5*
B-value (Å²)	
Protein	*40.8*
Ion/Ligand	*83*
Water	*38*
All atoms	*50.8*
Wilson plot B-value (Å²)	*45.8*
RMSD from ideal stereochemistry	
Bond lengths (Å)	*0.017*
Bond angles (°)	*1.88*
Coordinate error (Maximum-Likelihood Base) (Å)	*0.12*
Ramachandran plot (%)	
Most favored regions	*92.3*
Additional allowed regions	*4.8*
Disallowed regions	*2.9*

[1] $R_{sym}=\Sigma_i \Sigma_{hkl} |I_i(hkl)–(I(hkl)| \Sigma_{hkl} \Sigma_i I_i (hkl)$, where $I_i(hkl)$and $(I(hkl))$ represent the diffraction-intensity values of the individual measurements and the corresponding mean values. The summation is over all unique measurements.

[2] R_{meas} is a redundancy-independent version of R_{sym}, $R_{meas} = \sum_h \sqrt{n_h/n_h–1} \sum^{nh}{}_i | \hat{I}_h–I_{h,i}| / \sum_h \sum^{nh}{}_i I_{h,i}$, where $\hat{I}_h=1/n_h \sum^{nh}{}_i Ih, i$.

3. Results and discussion

3.1. Co-expression between a heterologous enzyme and E-PPase host enzyme

During the initial attempts to establish a protocol for expressing and purifying recombinant enzyme *Lv*Trx [13], high levels of the overexpressed *Lv*Trx were not found among the presence of *E. coli* proteins as a result of the long incubation period. After the ion exchange chromatography step had been performed, a denaturing electrophoresis (15% SDS-PAGE) was applied, revealing different protein populations and proportions (Figs. 1a, 1b).

During the purification process and despite several attempts to

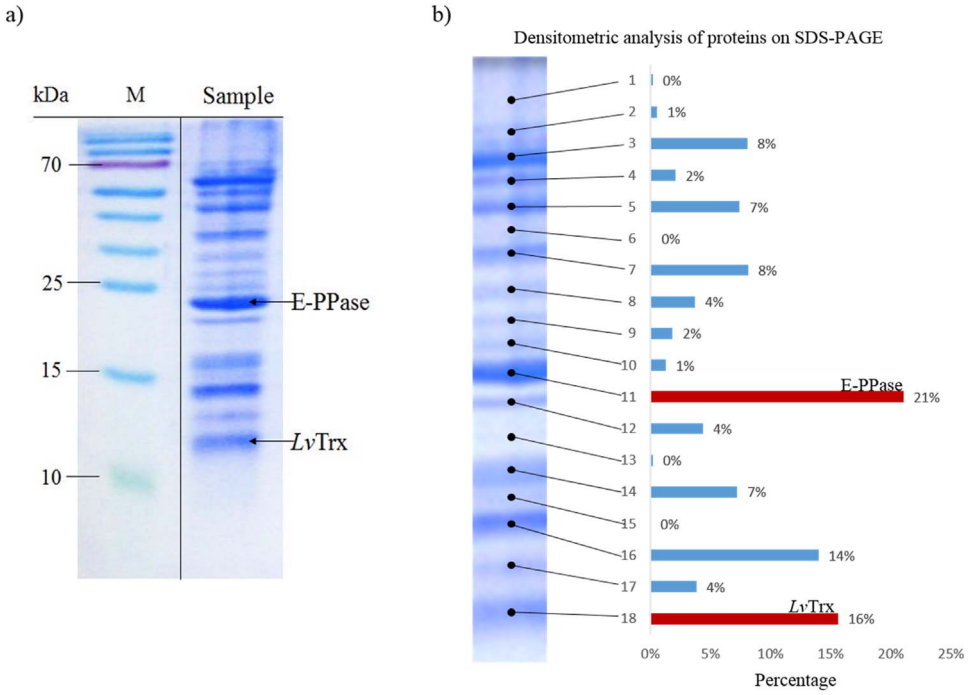

Fig. 1. a) Coomassie blue stain of SDS-PAGE of the sample that was crystallized. The first lane shows the markers (M). The second lane shows the non-homogenous sample used for crystallization trials. The arrows indicate the identification of the *Lv*Trx and E-PPase enzymes according to their molecular mass (12 kDa and 20 kDa, respectively). b) The relative concentration of *Lv*Trx and E-PPase were estimated using a densitometric analysis of the SDS-PAGE sample band profile. The densitometric analysis was performed by using the program ImageJ [21].

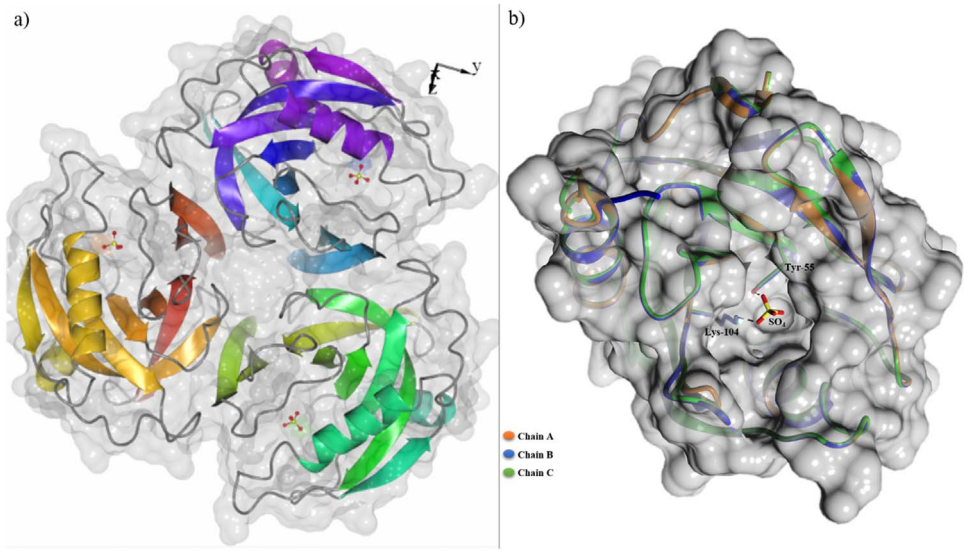

Fig. 2. a) E-PPase trimer complexed with SO_4^{-2} in ribbon representation. b) Superposition of chain A, B and C, showing the SO_4^{-2} bound to the E-PPase. The images were generated by CCP4mg and PDBsum, respectively [31,32].

improve it, we were unable to obtain a homogeneous sample. Therefore, we decided to perform crystallization trials with the sample as it was, which resulted in the E-PPase crystallization (after this experiment the conditions to effectively over-express *Lv*Trx were obtained and published) [13]. A densitometric analysis of the SDS-PAGE band profile presented in Fig. 1b estimates that 21% and 16% of the sample used for crystallization correspond, respectively, to E-PPase and *Lv*Trx. Additionally, E-PPases and *Lv*Trx are 2 among 18 species which generate a discrete band in the SDS-PAGE profile.

A likely explanation for why the E-PPase was favored throughout the expression, purification, and the crystallization process is that the purification protocol of E-PPase is very similar to the protocol for recombinant *Lv*Trx, specifically the heating step and ammonium sulfate precipitation steps [22]. Taking into account that the purification protocol of E-PPase requires 12 h for over-expression, this may explain the co-expression with the recombinant *Lv*Trx because 12 h of expression was, in fact, an additional stress condition for the bacterial culture. This long expression time reminds us that E-PPase is a constitutively expressed protein that plays an important role in macromolecular biosynthesis under stress conditions and is essential for the viability of *E. coli* in the last stages of bacterial culture [11,23].

During the purification protocol of the recombinant *Lv*Trx, the sample was heated to a temperature of 343 K for 20 min. At this temperature the *Lv*Trx protein is stable, but it is also known that the active conformation of bacterial PPases is stabilized by interactions between monomers in a hexameric arrangement, being the thermo-

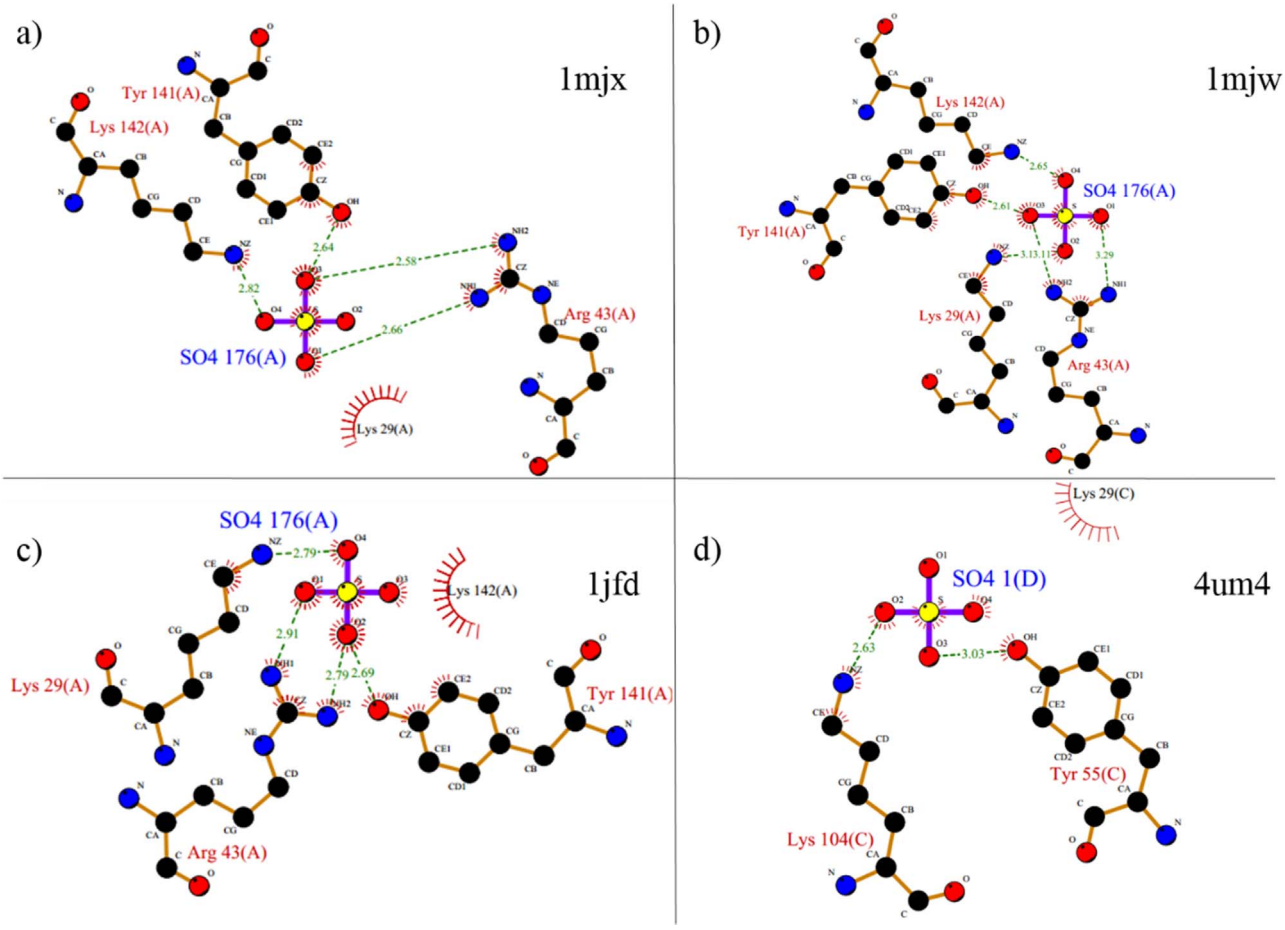

Fig. 3. a-c) Representation of SO_4^{-2} interactions among the E-PPases reported in the PDB (entries1mjx, 1mjw, 1jfd). d) E-PPase structure derived in this work (PDB entry 4um4) showing a different position of SO_4^{-2} interacting with residues Lys-104 and Tyr-55 at 2.6 Å and 3.0 Å, respectively. Figure prepared with LigPlot [35].

stability of bacterial PPases a primary property of the oligomer [24,25]. Thus, the E-PPase is stable at 343 K, maintaining *Lv*Trx and the E-PPase structurally stable during the purification process. Furthermore, it has been shown that E-PPase is a common contaminant enzyme in expression assays [26,27]. Retrospectively, including a gel filtration purification step could help to separate the hexameric E-PPase from the dimeric *Lv*Trx.

In regards to the crystallization process, the reported crystallization condition for recombinant *Lv*Trx [13] is very similar to those for E-PPase, potentially resulting in the favoring of the nucleation and crystal formation process of E-PPase more than *Lv*Trx due to E-PPase thermal stability and probably also because E-PPase represent the highest population, 21% of the total sample, among 18 species detected in the SDS-PAGE profile of the sample used for crystallization (Fig. 1b). Our results in other published works [12,13] conclude that the incubation time for the over-expression of *Lv*Trx was key in obtaining the recombinant enzyme completely pure (5 h instead of 12 h), without the presence of the E-PPase.

3.2. Molecular replacement and refinement

Originally, we were unable to determine the crystal structure of *Lv*Trx with the X-ray diffraction data collected and described in this work. After we successfully determined the crystal structure of *Lv*Trx [13], we decided to go back to the X-ray diffraction data described here. At initial stages of the phase determination process by MR using R 3 2 or H 3 2 as a space group, no solution could be found using the *Lv*Trx recombinant enzyme coordinates, even after trying different unit cell parameters, and space groups (P 1; C 2; R 3 or H 3) or other average search coordinate tricks (such as partial or multiple coordinates, use of poly-Ala or poly-Gly models, among several approaches). After failing with several trials of MR and exhausting all possible combinations using the *Lv*Trx coordinates for phase determination, we decided to consider that the crystallized protein could be another one coming from *E. coli*.

As an approximation to identify the protein, we decided to use the space group H 3 2, due to the apparent better statistics concerning the other space groups and unit cell candidates attempted while using *Lv*Trx coordinates.

The amplitudes from space group H 3 2 and the sequence from *Lv*Trx (sequence reference from UniProtKB was B1PWB9) were submitted to the CCP4i *BALBES* interface server, which found a solution structure by MR without user intervention [28]. The best solution found by *BALBES* was using the PDB coordinates from entry 1mjw [29] with a space group H 3 2 and refinement R_{work}/R_{free} values of 35/42%, which correspond to the inorganic pyrophosphatase from *E. coli*. In fact, if we had not reduced the data in the space group H 3 2 and used it in *BALBES*, we would not have been able to estimate the phases as readily. After the MR solution had appeared, we were able to corroborate that approximately 95% of the crystallographic structures of E-PPases deposited in the PDB belong to space group H 3 2, with unit cell parameters very similar to the parameters determined in this work.

The initial phases were obtained using the E-PPase coordinates from *E. coli* as the best search model. However, the parameters of the MR process resulted in a solution demonstrating an overlapping between the crystallographic neighbor copies. To address the problem, we used all the possible combinations of space groups and unit cell

parameters determined previously in this work. The best solution belonged to space group C 1 2 1, with unit cell parameters a =120.0 Å, b=108.9 Å, c=81.0 Å; α=90.0°, β=97° and γ=90.0°. Additionally, POINTLESS [30] clearly supported the final space group selection. It is important to remark, that space group C 1 2 1, is a novel space group for E-PPases. The final model of the E-PPase consisted of a trimer in the asymmetric unit in complex with SO_4^{-2} located in each monomer active site at 2.65 Å resolution (Table 1 and Figs. 2a, 2b).

3.3. E. coli *PPase crystal structure*

The crystal asymmetric unit contained three subunits, each including 175 amino acid residues with all the residues clearly visible in the final electron density map ($2F_o–F_c$ map). The biological hexamer is generated using crystallographic symmetries. In the active site crevice, we found fourteen amino acids residues limiting the cavity: Asp-42, Asp-65, Asp-67, Asp-70, Asp-97, Asp-102, Glu-20, Glu-31, Arg-43, Lys-29, Lys-104, Lys-142, Tyr-55 and Tyr-141. All these amino acid residues are also involved in binding Mg^{+2} ions [33]. However, the structure presented here does not have metal ions bound as shown in previously determined structures for *E. coli* PPase [34].

The three-dimensional structure of E-PPase at 2.65 Å resolution shows the presence of a sulfate ion bound to the active site of each of the three copies found in the asymmetric unit. These sulfate ions were previously reported bound to E-PPases PDB entries 1jfd at 2.20 Å, 1mjw at 1.95 Å and 1mjx at 2.15 Å [29,34]. The coordinates presented in this work show the different position and residue interactions of SO_4^{-2} (Lys-104, Tyr-55 and Lys-29) in comparison to the previously reported structures (Lys-29, Arg-43, Lys-142, and Tyr-141) mentioned above, probably because of the absence of Mg^{+2} ions (Fig. 3a-c).

In summary, a clear solution was found for the E-PPase structure by obtaining a trimer in the asymmetric unit with final refinement R_{work}/R_{free} values of 19.3/23.5%, indicating that this structure is closely related to the other E-PPases previously reported and deposited at PDB, with the only difference being in the SO_4^{-2} position and an increase of 100 $Å^3$ in the volume of the active site cavity in comparison with PDB entry 2auu which has Mg^{+2} ions bound (volume calculated in Mole Server) **(**Fig. 3d) [36].

4. Conclusion

This article highlights how the presence of different proteins in a sample used to set up crystallization experiments may favor the growth of crystals from a non-expected protein. However, while it is known that the use of non-homogeneous samples compromises the crystallization process, this work emphasizes how the use of every program or approach available, such as the search of MR models mining the PDB based on the unit cell parameters, as is implemented in *BALBES* [28], is pivotal to find solutions in extreme protein crystallography structure determinations when an unknown model actually exist in the PDB. Finally, at least with the data generated in this work, a sample which represents 21% of the total protein used for crystallization is capable of crystallizing. If we generalize this observation, it is likely to consider that to ensure the crystallization of a specific protein in the correct conditions; this protein needs to represent at least 80% of the total sample used for crystallization.

Acknowledgements

Campos-Acevedo, A. A. was supported by a PhD. fellowship from CONACyT. This work was funded by Grants CONACyT project No. 102370 and PAPIIT IN109114 to E. Rudiño-Piñera. We thank the staff at CCP4/APS School in Macromolecular Crystallography: From data collection to structure refinement and beyond (2012). We thank the staff at NSLS beamline X6A for data-collection facilities at Brookhaven National Laboratory. Beamline X6A is funded by NIGMS (GM-0080) and the US Department of Energy (No. DE-AC02-98CH10886). Authors thank Sonia G. Parra for critical reading of the manuscript and Sonia P. Rojas for technical assistance.

Transparency document. Supporting information

Transparency data associated with this article can be found in the online version at http://dx.doi.org/10.1016/j.bbrep.2016.09.011.

References

[1] A.M. Brzozowski, J. Walton, Clear strategy screens for macromolecular crystallization, J. Appl. Crystallogr. 34 (2001) 97–101.
[2] E. Saridakis, N.E. Chayen, Systematic improvement of protein crystals by determining the supersolubility curves of phase diagrams, Biophys. J. 84 (2003) 1218–1222.
[3] M. Hiraki, R. Kato, M. Nagai, T. Satoh, S. Hirano, K. Ihara, N. Kudo, M. Nagae, M. Kobayashi, M. Inoue, et al., Development of an automated large-scale protein-crystallization and monitoring system for high-throughput protein-structure analyses, Acta Crystallogr. D Biol. Crystallogr. 62 (2006) 1058–1065.
[4] N.E. Chayen, E. Saridakis, Protein crystallization: from purified protein to diffraction-quality crystal, Nat. Methods 5 (2008) 147–153.
[5] B. Lorber, D. Kern, H. Mejdoub, Y. Boulanger, J. Reinbolt, R. Giegé, The microheterogeneity of the crystallizable yeast cytoplasmic aspartyl-tRNA synthetase, Eur. J. Biochem. 417 (1987) 409–417.
[6] M. Skouri, B. Lorber, R. Giegé, J.-P. Munch, J.S. Candau, Effect of macromolecular impurities on lysozyme solubility and crystallizability: dynamic light scattering, phase diagram, and crystal growth studies, J. Cryst. Growth 152 (1995) 209–220.
[7] A. Moreno, A. Théobald-Dietrich, B. Lorber, C. Sauter, R. Giegé, Effects of macromolecular impurities and of crystallization method on the quality of eubacterial aspartyl-tRNA synthetase crystals, Acta Crystallogr. D Biol. Crystallogr. 61 (2005) 789–792.
[8] J.M. Van der Laan, M.B.A. Swarte, H. Groendijk, W.G.J. Hol, J. Drenth, The influence of purification and protein heterogeneity on the crystallization of p-hydroxybenzoate hydroxylase, Eur. J. Biochem. 179 (1989) 715–724.
[9] C.A. Kors, E. Wallace, D.R. Davies, L. Li, P.D. Laible, P. Nollert, Effects of impurities on membrane-protein crystallization in different systems, Acta Crystallogr. D Biol. Crystallogr. 65 (2009) 1062–1073.
[10] E. Niedzialkowska, O. Gasiorowska, K.B. Handing, K.A. Majorek, P.J. Porebski, I.G. Shabalin, E. Zasadzinska, M. Cymborowski, W. Minor, Protein purification and crystallization artifacts: the tale usually not told, Protein Sci. 3 (2016) 720–733.
[11] P.M. Burton, D.C. Hall, J. Josse, Constitutive inorganic pyrophosphatase of *Escherichia coli*. IV. Chemical studies of protein structure, J. Biol. Chem. 245 (1970) 4346–4352.
[12] E. Aispuro-Hernandez, K.D. Garcia-Orozco, A. Muhlia-Almazan, L. del-Toro-Sanchez, R.M. Robles-Sanchez, J. Hernandez, G. Gonzalez-Aguilar, G. Yepiz-plascencia, R.R. Sotelo-Mundo, Shrimp thioredoxin is a potent antioxidant protein, Comp. Biochem. Physiol. Part C 148 (2008) 94–99.
[13] A.A. Campos-Acevedo, K.D. Garcia-Orozco, R.R. Sotelo-Mundo, E. Rudiño-Piñera, Expression, purification, crystallization and X-ray crystallographic studies of different redox states of the active site of thioredoxin 1 from the whiteleg shrimp *Litopenaeus vannamei*, Acta Crystallogr. Sect. F Struct. Biol. Cryst. Commun. 69 (2013) 488–493.
[14] M.M. Bradford, A rapid and sensitive method for the quantitation of microgram quantities of protein utilizing the principle of protein-dye binding, Anal. Biochem. 72 (1976) 248–254.
[15] W. Kabsch, XDS, Acta Crystallogr. D Biol. Crystallogr. 66 (2010) 125–132.
[16] M.D. Winn, C.C. Ballard, K.D. Cowtan, E.J. Dodson, P. Emsley, P.R. Evans, R.M. Keegan, E.B. Krissinel, A.G.W. Leslie, A. McCoy, et al., Overview of the CCP4 suite and current developments, Acta Crystallogr. D Biol. Crystallogr. 67 (2011) 235–242.
[17] A.J. McCoy, R.W. Grosse-Kunstleve, P.D. Adams, M.D. Winn, L.C. Storoni, R.J. Read, Phaser crystallographic software, J. Appl. Crystallogr. 40 (2007) 658–674.
[18] G.N. Murshudov, A.A. Vagin, E.J. Dodson, Refinement of macromolecular structures by the maximum-likelihood method, Acta Crystallogr. D Biol. Crystallogr. 53 (1997) 240–255.
[19] P.D. Adams, P.V. Afonine, G. Bunkóczi, V.B. Chen, I.W. Davis, N. Echols, J.J. Headd, L.-W. Hung, G.J. Kapral, R.W. Grosse-Kunstleve, et al., PHENIX: a comprehensive Python-based system for macromolecular structure solution, Acta Crystallogr. D Biol. Crystallogr. 66 (2010) 213–221.
[20] P. Emsley, B. Lohkamp, W.G. Scott, K. Cowtan, Features and development of Coot, Acta Crystallogr. D Biol. Crystallogr. 66 (2010) 486–501.
[21] C.A. Schneider, W.S. Rasband, K.W. Eliceiri, NIH Image to ImageJ: 25 years of image analysis, Nat. Methods 9 (2012) 671–675.
[22] S.C.K. Wong, D.C. Hall, J. Josse, Constitutive inorganic pyrophosphatase of *Escherichia coli*. III. Molecular weight and physical properties of the enzyme and its subunits, J. Biol. Chem. 245 (1970) 4335–4345.
[23] J. Chen, A. Brevet, M. Fromant, F. Lévêque, J.M. Schmitter, S. Blanquet, P. Plateau, Pyrophosphatase is essential for growth of *Escherichia coli*, J. Bacteriol. 172 (1990) 5686–5689.
[24] J. Kankare, G.S. Neal, T. Salminen, T. Glumoff, T. Glumoff [corrected to T.

Glumoff], B.S. Cooperman, R. Lahti, A. Goldman, The structure of *E.coli* soluble inorganic pyrophosphatase at 2.7 A resolution, Protein Eng. 7 (1994) 823–830.
[25] T. Salminen, A. Teplyakov, J. Kankare, B.S. Cooperman, R. Lahti, A. Goldman, An unusual route to thermostability disclosed by the comparison of *Thermus thermophilus* and *Escherichia coli* inorganic pyrophosphatases, Protein Sci. 5 (1996) 1014–1025.
[26] S. Benini, G. Degrassi, I. Krastanova, D. Lamba, V. Venturi, Purification, crystallization and preliminary X-ray analysis of an acetylxylan esterase from *Bacillus pumilus*, Acta Crystallogr. D Biol. Crystallogr. D57 (2001) 1906–1907.
[27] S. Benini, G. Degrassi, I. Krastanova, D. Lamba, V. Venturi, Purification, crystallization and preliminary X-ray analysis of an acetylxylan esterase from *Bacillus pumilus*. *Er*, Acta Crystallogr. D Biol. Crystallogr. D60 (2004) 1346.
[28] F. Long, A.A. Vagin, P. Young, G.N. Murshudov, *BALBES*: a molecular-replacement pipeline, Acta Crystallogr. D Biol. Crystallogr. 64 (2008) 125–132.
[29] S.M. Avaeva, E.V. Rodina, N.N. Vorobyeva, S.A. Kurilova, T.I. Nazarova, V.A. Sklyankina, V.Y. Oganessyan, E.H. Harutyunyan, Changes in *E. coli* inorganic pyrophosphatase structure induced by binding of metal activators, Biochemistry 63 (1997) 592–599.
[30] P. Evans, Scaling and assessment of data quality, Acta Crystallogr. D Biol. Crystallogr. 62 (2006) 72–82.
[31] S. McNicholas, E. Potterton, K.S. Wilson, M.E.M. Noble, Presenting your structures: the CCP4mg molecular-graphics software, Acta Crystallogr. D Biol. Crystallogr. 67 (2011) 386–394.
[32] T.A.P. De Beer, K. Berka, J.M. Thornton, R.A. Laskowski, PDBsum additions, Nucleic Acids Res. 42 (2014) D292–D296.
[33] E.H. Harutyunyan, V.Y. Oganessyan, N.N. Oganessyan, S.M. Avaeva, T.I. Nazarova, N.N. Vorobyeva, S.A. Kurilova, R. Huber, T. Mather, Crystal structure of holo inorganic pyrophosphatase from *Escherichia coli* at 1.9 A resolution. Mechanism of hydrolysis, Biochemistry 36 (1997) 7754–7760.
[34] S. Avaeva, S. Kurilova, T. Nazarova, E. Rodina, N. Vorobyeva, V. Sklyankina, O. Grigorjeva, E. Harutyunyan, V. Oganessyan, K. Wilson, et al., Crystal structure of *Escherichia coli* inorganic pyrophosphatase complexed with SO_4^{2-}, Ligand-induced molecular asymmetry, FEBS Lett. 410 (1997) 502–508.
[35] R.A. Laskowski, M.B. Swindells, LigPlot+: multiple ligand-protein interaction diagrams for drug discovery, J. Chem. Inf. Model 51 (2011) 2778–2786.
[36] D. Sehnal, R. Svobodová Vařeková, K. Berka, L. Pravda, V. Navrátilová, P. Banáš, C.M. Ionescu, M. Otyepka, J. Koča, MOLE 2.0: advanced approach for analysis of biomacromolecular channels, J. Cheminform. 5 (2013).